Nanoscale diffusion in Pt/^{56}Fe/^{57}Fe thin-film system

A. Tynkova [a,b], G.L. Katona [a,*], G. Erdélyi [a], L. Daróczi [a], A.I. Oleshkevych [b], I.A. Vladymyrskyi [b], S.I. Sidorenko [b], S.M. Voloshko [b], D.L. Beke [a]

[a] University of Debrecen, Department of Solid State Physics, H-4010 Debrecen, P.O. Box 2, Hungary
[b] National Technical University of Ukraine 'Kyiv Polytechnic Institute' Peremogy av. 37, Kyiv, 03056, Ukraine

A B S T R A C T

Low-temperature diffusion of Fe in Pt/^{56}Fe/^{57}Fe thin films (grown on MgO (100) substrate) was investigated between 703 K and 813 K using secondary neutral mass spectrometry. The activation energy of the effective interdiffusion coefficients, evaluated by the "centre-gradient" method, is 1.53 ± 0.25 eV reflecting a strong contribution from grain boundaries. This is also supported by the observed deep penetrations of Pt into the ^{56}Fe layer, from which the grain boundary diffusion coefficients for Pt in Fe were also estimated and 1.45 ± 0.25 eV activation energy was obtained. A simple model, including the effect of grain boundaries to the overall intermixing at the original sharp interfaces in nanocrystalline films, is developed. This predicts that at short annealing times the grain boundary diffusion dominates, and bulk diffusion coefficients can be determined only in long time limit. At intermediate annealing times, when the grain boundaries are saturated but the bulk diffusion is still negligible, there are no changes in the composition profiles. This yields good qualitative agreement with the experimental data and offers explanation for the time and temperature dependence of the interdiffusion coefficients obtained in similar systems.

© 2015 Elsevier B.V. All rights reserved.

1. Introduction

The knowledge of diffusion in nanostructures at low temperatures is very important for understanding their thermal stability and many materials properties [1–3]. Besides bulk diffusion, structural defects (triple junctions, grain boundaries or dislocations) – as diffusion short circuits — can also provide important contribution to any material rearrangement like grain growth and structural relaxation. Thus, even if the considerations are restricted to pure materials, the mechanisms of grain growth, relaxation and defect annihilation at low temperatures can only be understood on the basis of the understanding of the role of these different contributions. Furthermore, the minimum volume diffusion penetration length (equal to $2\sqrt{D_V t}$, where D_V is the bulk diffusion coefficient and t is the annealing time), determined by classical (like radiotracer) methods is usually not less than 10–20 nm, which can be larger or in the same order of magnitude as the grain size. More recently publications on diffusion in isotope bi- or multilayered systems indicated that it is possible to investigate, with the use of sophisticated techniques like neutron reflectivity in isotope multilayers [4] or nuclear resonant scattering of synchrotron radiation [5], diffusion intermixing even on bulk diffusion lengths in the order of 0.5-1 nm. At these penetration distances, in epitaxial structures or in stable nanostructures with grain sizes several times larger than the bulk penetration distance, it would be expected the grain boundary contributions can be excluded. This would mean that the effective diffusion coefficients correspond to bulk diffusion. As we will see below these investigations [4,5], although provided very interesting results, raised also questions related to the surprisingly low activation energy and time dependence of the effective diffusion coefficients. Thus, in this communication, on the basis of experiments carried out by depth profiling on ^{56}Fe/^{57}Fe thin films, we provide a simple model for the interpretation of the time dependence of the effective diffusion coefficients obtained at fixed temperatures.

Self-diffusion of iron in the bulk has been studied widely and there are reliable experimental data over a wide temperature range [6–12]. According to the selected data collection [13], the activation energy, Q, is 2.92 eV in the 783-1017 K temperature range in the bulk Fe (α - phase).

Several papers describe Fe self-diffusion experiments in thin films (e.g. FeN$_{0.7}$, FeZr, FePt) using secondary ion mass-spectrometry (SIMS), as well as grazing-incidence nuclear resonant scattering of synchrotron radiation [5,14–16]. For example, in Ref. [5] self-diffusion of Fe in Pt(2 nm)/^{57}FePt (2 nm)/FePt(3 nm)$_{10}$ multilayers on (001) MgO substrate at low temperatures (773 K and 873 K) was studied. The annealing times were between 60 and 120 minutes and the Fe diffusivities were found in the range of 10^{-22} -10^{-24} m^2 s^{-1}. The activation energy was (1.65 ± 0.29) eV. Such a small value would suggest a significant contribution from grain boundary diffusion. However, in the discussion of Ref. [5] the authors argued, that real low temperature bulk diffusion

* Corresponding author. Tel.: +36 52 316073.
  E-mail address: gabor.katona@science.unideb.hu (G.L. Katona).

was observed with a highly correlated mechanism in the chemically ordered FePt phase. Nevertheless, as it was mentioned in the discussions, contributions from grain boundaries could not be fully excluded.

In addition, it was demonstrated in Ref. [4] that Fe self-diffusion can be investigated in ^{57}Fe(7 nm)/^{nat}Fe(3 nm)$_{15}$ multilayers at low temperatures using neutron reflectivity experiments. Chakravarty et al. [4] argued that they could diminish the grain boundary contributions since no significant grain growth during heat treatments was observed. It was concluded that, according to the Harrison's classification [17], B-type diffusion regime was implemented in which both the bulk and grain-boundary diffusion contribute to the intermixing. Interestingly, a remarkable time dependence of the effective diffusivities was observed and after very long annealing times the diffusivities, obtained above 673 K, were in good agreement with those measured in the bulk of single crystals. On the other hand, the activation energy deduced from the data obtained at short (20 min) annealing times was about 1 eV. Chakravarty et al. [4] concluded that due to the small bulk diffusion lengths (~1 nm), the role of grain boundaries could be neglected and point defect annealing processes at around the initial interfaces can explain the observed time dependence of the effective diffusion coefficient.

Simultaneous determination of bulk and grain-boundary (GB) self-diffusion coefficients of Fe in polycrystalline films has been described [18] in ^{56}Fe/^{57}Fe bilayers. The average film thicknesses were about 100 nm. The samples were annealed at 443 K and 463 K for 5 and 18 min in order to determine Fe self-diffusion. Calculations of the bulk, D_v and grain-boundary, D_{gb} self-diffusion coefficients of iron were based on SIMS data: the values were $D_v \sim 10^{-21}$ m^2 s^{-1} and $D_{gb} \sim 10^{-17}$ m^2 s^{-1}, respectively.

The above examples illustrate that the details on the contribution of different diffusion mechanisms to the overall intermixing are not well-understood in nanosystems if the bulk diffusion distance is in the order of 0.5-5 nm. In modern methods, based e.g. on neutron reflectivity in isotope multilayers[4] or nuclear resonant scattering of synchrotron radiation [5] it is possible to investigate diffusion intermixing even on bulk diffusion lengths in the order of 1 nm. On the other hand these, or similar methods are usually based on the determination of the average decay of an initially sharp interface. Thus it is a relevant general question: do grain boundaries (if present) contribute to this intermixing on the above mentioned very short distances? If yes, what is the contribution of GBs to the effective diffusion coefficients? We address this question in this communication via investigation of diffusion intermixing in ^{56}Fe/^{57}Fe isotope bilayer using depth profiling by a Secondary Neutral Mass Spectrometer (SNMS), which provides a very good depth resolution and even about 1-2 nm [19–22] can be reached. Additionally, we interpret our results by means of a model calculation in a bilayer structure having GBs perpendicular to the interface.

The role of oxidation in modifying diffusion in thin films has been discussed by several authors [23–25], and on the basis of these works one can suppose that the enhanced diffusion along GBs of the ^{57}Fe/^{56}Fe layer may be due to the influence of the oxidation process of ^{57}Fe on the outer surface, which creates an additional driving force for diffusion.

Thus, the grain boundary diffusion and oxidation are two factors that can have a significant effect on the rate of the self-diffusion in thin films with nanometer dimensions and can lead to serious difficulties in the interpretation of data obtained. Our primary aim was to investigate Fe self-diffusion in epitaxial thin films Pt/^{56}Fe/^{57}Fe on the (100) surface of MgO crystals. Epitaxially grown films were chosen since we wanted to diminish the effect of GBs. Furthermore, Pt cap layer was deposited on the top surface in order to eliminate the oxidation process although an interaction between the Pt and Fe is expected since intermetallic phases can be formed. Thus the ^{56}Fe layer was selected to be much thicker than the ^{57}Fe layer. In the evaluation of the measured composition profiles after interdiffusion, the well-known 'centre-gradient'- or the Hall-Morabito 'middle of the gradient' - method [26, 27] was used.

2. Experimental details

The Pt/^{56}Fe/^{57}Fe on MgO(100) films were prepared as follows: ^{56}Fe and ^{57}Fe layers were sequentially deposited by molecular beam epitaxy and the upper layer of Pt was produced by magnetron sputtering. The vacuum in the chamber was 10^{-8} Pa. For the preparation of the ^{56}Fe-rich and ^{57}Fe-rich films the following iron targets were used: i) target with natural abundance of ^{56}Fe (91.68 at%) and ii) target with ^{57}Fe (94.7 at%). Composition of the samples is presented in Table 1. The composition of ^{57}Fe was determined by mass spectrometry method.

To confirm the epitaxial growth of the layers, the structure was investigated by X-ray diffraction using a Bruker D8 diffractometer with Cu$_{K\alpha}$ radiation. Diffraction data were collected using a θ-2θ scan mode. The results are given in Fig. 1. These data show that only the (200) peaks of Fe are present indicating that the film has a texture with orientation perpendicular to the substrate surface. The structure was also investigated by X-ray diffraction in a grazing incidence geometry using a Siemens D5000 diffractometer with Cu$_{K\alpha}$ radiation. A parallel beam was provided by an X-ray mirror. Diffraction data were collected with a constant angle of the incident beam, 3°, using a 2θ scan mode. These data show, as expected, one peak of Fe for the (200) spacing when the substrate is appropriately oriented. The data, collected for different orientations, indicate the good quality of the film with the expected orientation.

The thicknesses of the layers were determined by X-ray reflection (Fig. 2) using a Philips PW3830 diffractometer with Cu$_{K\alpha}$ radiation and a graphite monochromator in front of the detector. Two calibration samples of ^{56}Fe and ^{57}Fe have been prepared and measured by X-ray reflectivity in order to determine the deposition rate. This allowed the estimation of the thickness of ^{56}Fe and ^{57}Fe films from the separation of the fringes [28]. The difference between the critical angle θ$_c$ and the fringe labeled as θ$_{Pt}$ allows us to determine the thickness of Pt layer. The calculated thicknesses of the Pt and combined ^{56}Fe and ^{57}Fe layers were 12±1 nm and 90.0±0.4 nm, respectively. Given that the rates of deposition for ^{56}Fe and ^{57}Fe were determined from the calibration samples we deduce that the thicknesses of the Pt, ^{56}Fe and ^{57}Fe layers are 12 nm, 65 nm and 25 nm respectively.

Diffusion experiments were made on pieces cut from the as received samples providing identical films for annealing at several different temperatures. The composition-depth profiles of the samples were determined by Secondary neutral mass spectrometry, SNMS (type INA-X from SPECS GmbH, Germany). Low-pressure Ar$^+$ plasma was used as both bombarding ion source and post-ionization medium. Ar$^+$ ions were directed to the sample surface by applying a negative voltage to the sample. The diameter of the sputtering area was fixed as 3 mm. Concentration of elements was calculated using relative sensitivity factors assuming a linear dependence of the corrected intensities on compositions.

The annealing time was 900 s at each temperature to allow comparison with the results of Chakravarty [4] and Vasylyev [18]. During this time, the diffusion became observable at 773 K and complete intermixing was found at 873 K. Two additional temperatures (813 K and 843 K), were selected in order to determine the activation energy.

3. Results

Experimental data obtained from the SNMS depth profiles, i.e. the composition versus sputtering time curves, are shown in Fig. 3. It can

Table 1
Composition of Samples.

Sample	^{56}Fe-rich	^{57}Fe-rich
Isotope	at %	at%
^{54}Fe	5.84	0
^{56}Fe	91.68	3.14
^{57}Fe	2.17	94.7
^{58}Fe	0.31	2.16

be seen that after heat treatments both iron isotopes have segregated on the free surface of Pt. Furthermore, with increasing temperature the intermixing between the Pt and [56]Fe becomes more obvious at the place of the initial Pt layer. The high average composition of Fe in the centre of Pt layer, as seen in Fig. 3(e), corresponds to the 1:3 Fe/Pt ratio. Note that not only the [56]Fe penetrates into the Pt layer, but the [57]Fe penetration is also clearly visible. At the same time the Pt also penetrates into the [56]Fe layer. The Pt concentration gradually decreases from the Pt/[56]Fe interface indicating that during the applied heat treatments the [56]Fe layer was thick enough not to be saturated by Pt leading to negligible penetration of Pt into the [57]Fe layer.

It can also be seen in Fig. 3 that, with increasing temperature, there is an increasing intermixing between the isotope layers and the slope of the composition profile became less steep. At 873 K [57]Fe and [56]Fe atoms are homogeneously distributed throughout the entire thickness of the system. Interestingly the highest Pt concentration of about 20 at.% was observed just below the near surface region.

The effective Fe interdiffusion coefficient, D, describing the intermixing between the two layers at short annealing times, can be determined from the composition profiles obtained at the [56]Fe/[57]Fe interface by the so-called Hall-Morabito [26,27] or "centre-gradient" [29] method. This method takes into account the initial broadening of the profile of the as-deposited sample. This widening of the initial profile can be explained by different reasons: i) roughness of the initial interface, ii) intermixing already during the deposition process, iii) instrumental effects. Thus, the composition profile obtained after heat treatments can be considered as the convolution of the initial profile and the profile created by the diffusional intermixing process itself [29]. If the intermixing is described by only one composition independent effective diffusion coefficient, then the composition profile (arising from the diffusional intermixing) has the form of a complementary error function as

$$\frac{\overline{c}}{c_0} = \frac{1}{2} erfc \left[\frac{x}{2\sqrt{Dt}} \right], \tag{1}$$

where c_0 is the initial concentration at the interface, x is the distance from this interface and t is the annealing time. As it was discussed by Hall and Morabito [25] if the initial (in our case mainly instrumental) broadening of the profile can also be described approximately by an erfc function near the interface, than the interdiffusion coefficient can be calculated from the following formula:

$$D = \left(\frac{1}{G_T^2} - \frac{1}{G_0^2} \right) \frac{1}{4\pi t}, \tag{2}$$

where G_o and G_T are the concentration gradients at the original interface for the as-deposited and the annealed specimens, respectively. For the calculation of the concentration gradients the sputtering time scale was converted to depth scale assuming constant sputtering rate, 0.56 nm/s, estimated from the position of the 77 nm thick (Pt + [56]Fe) layer at 138 s [see Fig. 3(a)].

The values of the effective self-diffusion coefficients for Fe atoms, calculated from Eq. (2), are shown in Table 2 and in Fig. 4. It should be noted, that the presence of Pt at the Fe GBs (see later) means, that the contribution of GB diffusion to the overall intermixing is not pure Fe GB diffusion in pure Fe but Fe GB diffusion along Pt containing Fe GBs. However, as it is shown later the Fe self-diffusion along GBs is approximately equal to the GB diffusion of Pt in Fe, thus we assumed that practically the Fe self-diffusion was measured. The uncertainty of the diffusivities has been approximated from the uncertainty of the concentration gradients. A linear dependence is seen in the Arrhenius plot, with (1.53 ± 0.25) eV activation energy. The values for the diffusion coefficients lie in the range between data for the bulk diffusion in single crystals [6,8,9] and grain boundary diffusion in polycrystalline α-Fe [11]. This is a strong indication that, although we intended to produce epitaxial films free of grain boundaries, there should exists some short

circuits in our samples. Indeed, in accordance with the results of Ref. [4] (where columnar boundaries were present with a grain size of about 15 nm), it can be seen in Fig. 5 that there are tilt boundaries in our samples as well, and the grain size can be estimated to be between 10 and 30 nm. Thus it can be concluded that although in our case the deposition technique was different, columnar grains, all oriented parallel with the preferred orientation dictated by the MgO (100) substrate, have been formed too (see Fig. 5). This explains why we obtained a significant penetration of Pt into the Fe layer: indeed this should be explained by GB diffusion of Pt into the Fe. Plotting the logarithm of the Pt composition versus x^2, if we are in the C-type regime of grain boundary diffusion (i.e. when the atomic transport is restricted to GBs and bulk diffusion penetrations are negligible), straight line should be obtained [31]. From the slopes of these plots the Pt grain boundary diffusion coefficients can be estimated (Fig. 6). Their values are also included in Table 2.

It is important to note that in Fig. 3 similar penetration of [57]Fe into the [56]Fe layer is observed as for the Pt penetrations, see e.g. Fig. 3(c). Thus even the determination of the Fe grain boundary diffusion coefficients would be possible. However, the [56]Fe/[57]Fe interface lies at much deeper position from the initial interface as compared to the Pt/[56]Fe interface. It is necessary to take into account that during the SNMS depth profiling the shape of the crater created gradually deviates from the ideal cylindrical profile. Especially the bottom of the crater becomes progressively less flat causing an experimental smearing of depth profile even with a chemically or isotopically sharp interface. Thus the Pt/[56]Fe interface is much sharper than the [56]Fe/[57]Fe interface even in the as received state as seen in Fig. 3(a). As a second consequence the determination of the position of the [56]Fe/[57]Fe boundary and thus a plot similar to that of Pt penetration in Fig. 6 would have higher uncertainty, and a similar systematic evaluation of the profiles of grain boundary penetration of [57]Fe into the [56]Fe was not possible. Nevertheless from the [57]Fe composition distribution measured at 773 K - after subtracting the initial [57]Fe level, assuming again pure C-type regime and using similar plotting as in Fig. 6 - an order of magnitude estimate gives: $D_{gb}^{Fe \rightarrow Fe} = 1 \times 10^{-19}$ m[2] s^{-1}. This corresponds approximately to the Pt grain boundary diffusion coefficient at this temperature.

In the light of the above values obtained for the diffusion coefficients and activation energies we can conclude that these represent primarily atomic transport along tilt GBs. Estimating the bulk penetration depth for 900 s from the data of Lübbehausen and Mehrer [8] one obtains 1.7 nm at 843 K and 0.02 nm at 703 K, respectively. This indicates that the Pt diffusion into Fe is certainly in the C-type regime of GB diffusion (the value of $2\sqrt{D_v t}$ is less than the grain boundary thickness, $\delta = 0.5$ nm) at the two lowest temperatures, and in a transition region between B- and C-type regimes for the other two.
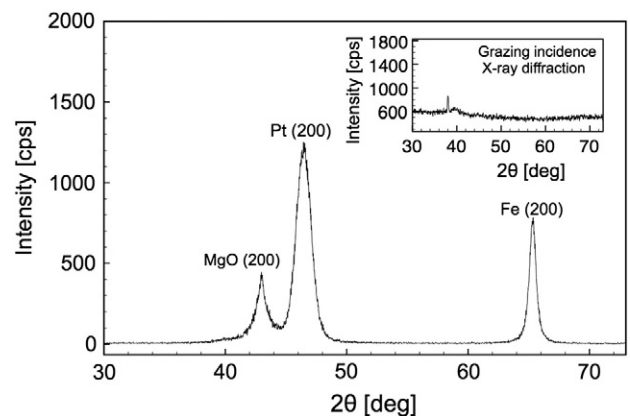

Fig. 1. X-ray diffraction pattern for the Pt/[56]Fe/[57]Fe as-deposited sample. The grazing incidence X-ray diffraction pattern is shown in the inset.
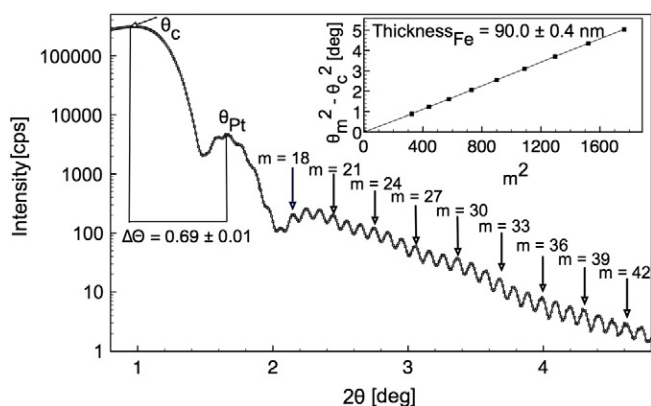
Fig. 2. X-ray reflectivity from as received Pt/^{56}Fe/^{57}Fe on the MgO (100) substrate. The measurements were carried out by Cu$_{K\alpha}$ radiation.

Table 2
Calculated diffusion coefficients for Fe interdiffusion and Pt grain boundary diffusion (second values for Pt diffusion coefficients were obtained after corrections: see the text).

T [K]	D^{Fe} [m^2 s^{-1}]	$D^{gb}_{Pt \to Fe}$, m^2 s^{-1} (GB)		$\frac{\delta}{2\sqrt{D_v t}}$	D_{app}/D_{tru}
		calculated values	values after correction		
703	7.6×10^{-22}	6.4×10^{-20}	6.4×10^{-20}	31.2	1
773	4.1×10^{-21}	1.4×10^{-19}	1.6×10^{-19}	5.88	0.9
813	5.9×10^{-21}	2.8×10^{-19}	5.6×10^{-19}	0.94	0.5
843	2.3×10^{-20}	6.0×10^{-19}	2.4×10^{-18}	0.3	0.25

in the annealing time. Both the GB diffusion coefficients, D_{gb}, and triple products, determined from this transition regime, contain systematic errors. According to Szabo et al. [32] (see Fig. 1 in Ref. [32]) these errors are the function of the $\alpha = \delta s/2(D_V)$ parameter. Assuming that the segregation coefficient of Pt is unity, at $\alpha = \delta/2(D_V t) = 0.3$, corresponding to the value of α belonging to 843 K, the grain boundary diffusion coefficient is underestimated by a factor of 2. At 813 K ($\alpha = 0.94$) and 773 K ($\alpha = 6$) this correction factor is about 1.7 and 1.1 respectively (shown in the last column of Table 2). Using these corrections the Arrhenius plot gives (1.45 ± 0.25) eV activation energy (see the corrected values in Table 2. as well as Fig. 4).
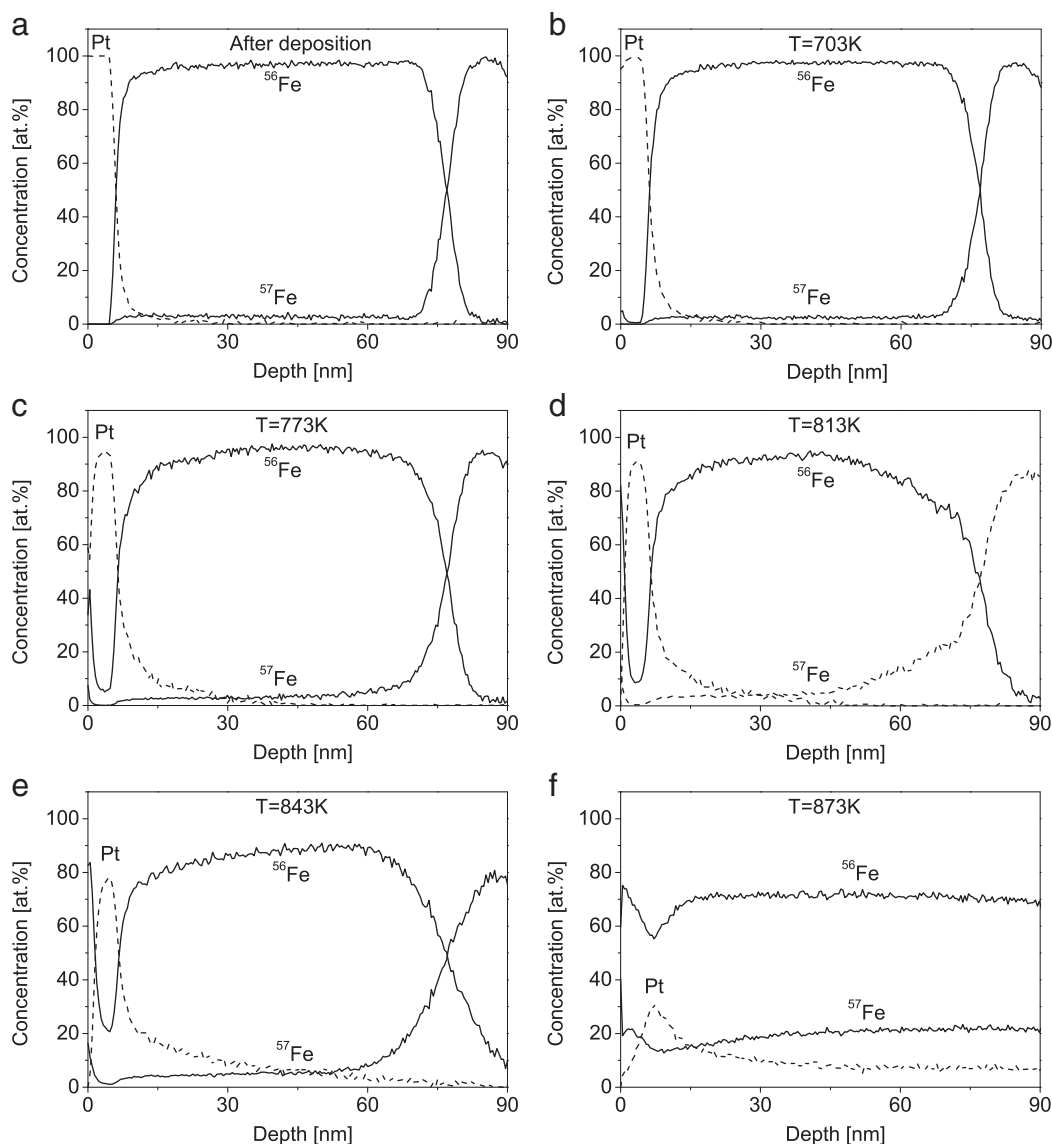
In the B-type regime both the GB and bulk diffusion contribute to the diffusion and from this the GB triple product, $\delta s D_{gb}$ can be determined (s is the segregation factor), if D_V is known [31]. Between the two regimes there is a (several orders of magnitude) wide transition regime

Fig. 3. Concentration distributions of the components in the Pt/^{56}Fe/^{57}Fe thin film system. (a) before and (b-f) after annealing at different temperatures for 900 s.
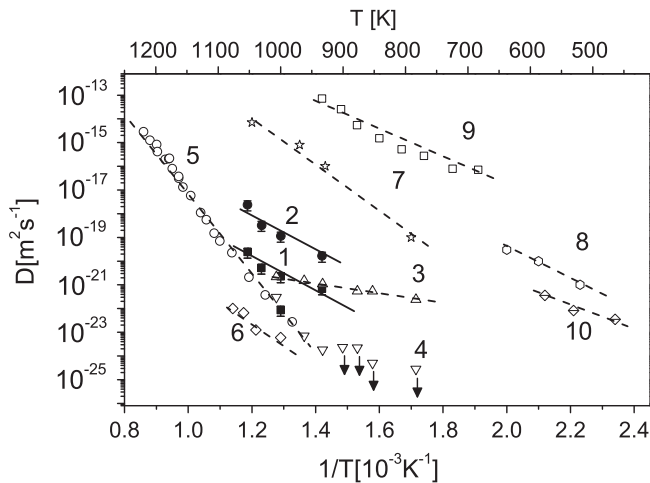
Fig. 4. Arrhenius plot for: 1. effective interdiffusion coefficients for Fe (present work); 2. grain-boundary diffusion coefficients for Pt into Fe layer (present work); 3. & 4. self-diffusivities in nanocrystalline Fe after 20 min and 230 h of annealing respectively (the arrows indicate upper limits) [4]; 5.volume diffusion in single crystals [8]; 6. Fe self-diffusion in Pt(2 nm)/^{57}FePt (2 nm)/FePt (3 nm)$_{10}$ multilayers system [5]; 7. α-iron self-diffusion along dislocations [30]; 8. C-type grain-boundary diffusion in nanocrystalline Fe with an unstable nanostructure [10]; 9. C-type grain-boundary diffusion in the coarse-grained Fe [11]; 10. grain-boundary self-diffusivities in nano-crystalline Fe [12].

Finally it is worth mentioning the formation of the near surface intermixed region (with approximate composition of FePt$_3$: see Fig. 3(e)), in the place of the original Pt layer instead at the original Pt/^{56}Fe interface. The formation of this inside the original Pt layer can be interpreted by the so-called grain boundary diffusion induced solid state reaction [33]. Furthermore, the observed minimum of the ^{56}Fe composition in Fig. 3(e) can be interpreted as rapid segregation of iron at the free surface: the saturation of the surface layer and the fast grain boundary diffusion initiate the formation of the new phase in the near surface region.

4. Discussion

The structure of our films is similar to the structure of the isotope multilayer used in Ref. [4], where columnar grains of about 10 to 20 nm diameter were observed. The only small difference was that in their case no significant texture was present, while in our case the film was strongly textured in the (200) direction being perpendicular to the substrate surface. This is why we identified the GBs in Fig. 6 as

Fig. 6. Penetration profiles for Pt into the Fe layer: logarithm of the concentration versus the square of the distance from the boundary.

tilt boundaries. Since the film structure is quite similar, if the Pt penetration profiles would not be observed, one would agree with the interpretation given in Ref. [4] for short annealing times: the relatively high effective diffusion coefficients, as compared to the extrapolated bulk values, are the result of the effect of extra defects created during the deposition process in the vicinity of the interfaces. In addition it was assumed in Ref. [4] that the contribution of grain boundary transport was not dominating and could be neglected. In contrast to this, our Pt penetration profiles clearly indicated a direct GB penetration into the ^{56}Fe layer and the activation energy of Pt grain boundary diffusion coefficients was nearly the same as the activation energy of the effective Fe self-diffusion. This indicates that in our case the GB transport in the effective Fe self-diffusion cannot be neglected.

Thus, we conclude that the Pt penetration profiles provide direct evidence that there is also a considerable simultaneous transport along
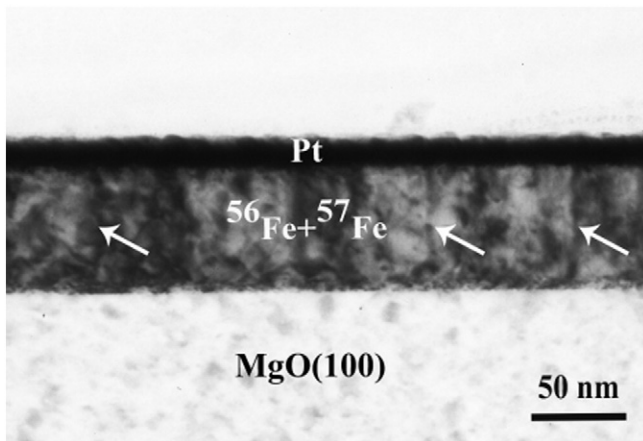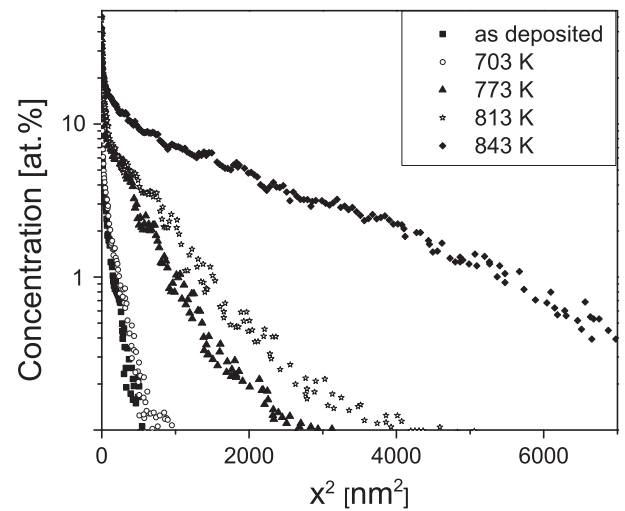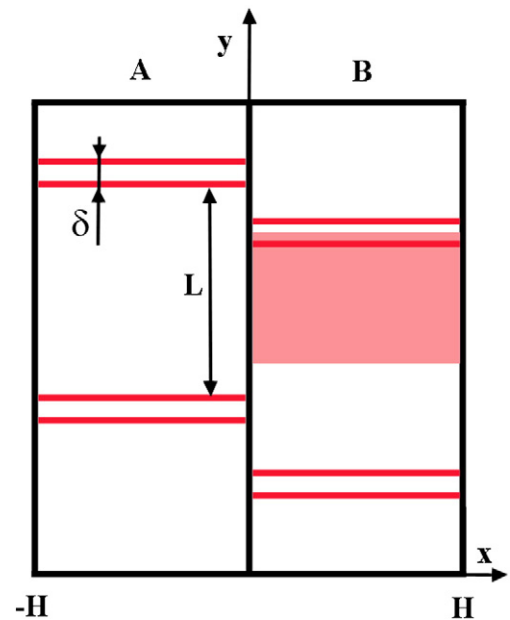

Fig. 5. Bright field TEM picture of the sample after annealing at 523 K for 15 min. the bottom (darker) part is the Pt layer. Arrows point some of the tilt boundaries oriented perpendicular to the substrate.

Fig. 7. Scheme of the two-dimensional model of an A/B nanocrystalline diffusion pair. H is the thicknesses of the films, L is the distance between the grain boundaries of δ thick. The interface is situated at $x = 0$. The shaded area corresponds to the unit cell used in the calculations (see also the text).
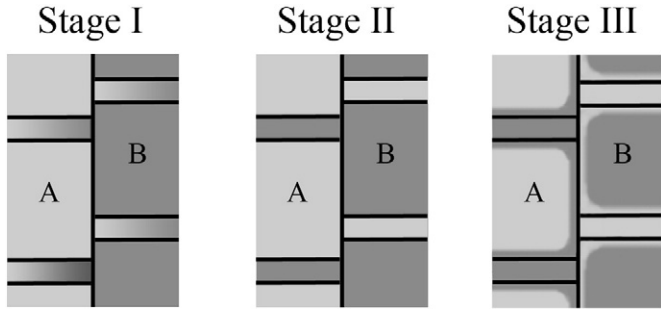
Stage I Stage II Stage III

Fig. 8. Different stages of composition distributions obtained at increasing annealing times during diffusion intermixing in an A/B binary nanostructure shown in Fig. 7 (see also the text).

GBs. The GBs can have also a time dependent influence on the effective diffusivities obtained by techniques sensitive to the change of the slope of the composition profiles at the position of the initial interface. These techniques are e.g. the neutron reflectivity [4], nuclear resonant scattering of synchrotron radiation [5] or SNMS used by us (via the centre-gradient method) for measuring Fe self-diffusion.

In order to make the above conclusions more solid, let us consider a qualitative model of parallel grain-boundaries, perpendicular to the original interface with spacing of a few nanometers (Fig. 7). It is expected that the material present in the GBs can also have a detectable contribution to the slope of the average concentration profile at the position of the initial interface, if the grain boundary fraction is larger than 5-10%. In addition, this contribution can be time dependent because at different annealing times the ratio of the areas filled by direct bulk as well as grain boundary diffusion can change (Fig. 8). Accordingly, the effective diffusion coefficient can have different contributions from the above two mechanisms at different annealing times. At short times (Stage I in Fig. 8) the effect of the material present in the GBs is dominating. At intermediate times, the composition in the GBs becomes homogeneous (Stage II in Fig. 8), there are still no bulk penetrations. Thus in this stage there will be practically no changes with increasing annealing time in the slope of the composition, averaged over the planes parallel with the initial interface. Finally at longer annealing times, when the bulk penetration distance is larger than the grain boundary width, δ, the bulk diffusion will be the dominating mechanism determining the slope (Stage III in Fig. 8). Obviously this picture can be refined according to the more complex defect structure of interfaces. For example, the presence of a dislocation network, perpendicular to interface can additionally be taken into account supposing an intermediate diffusivity between that in the bulk and that in GBs. Nevertheless, the qualitative picture remains the same.

In order to confirm the above qualitative conclusions we have carried out model calculations on the change of the slope of the composition profiles as a function of annealing time. We supposed a nanocrystalline A/B bilayer film (shown schematically in Fig. 7) with regularly spaced GBs. The GBs were separated by the distance L and they were perpendicular to the plane of the film and to the interface as well. It was supposed that in the individual thin films both the volume and grain boundary diffusion coefficients were concentration independent and the corresponding coefficients were the same in both layers. This last assumption is indeed fulfilled in our samples for Fe diffusion.

The GBs are considered as 3D slabs (slab width δ=0.5 nm), their depth is determined by the sample lateral dimension in direction z, (perpendicular to x-y plane in the Fig. 7). In the following calculations this dimension can be chosen arbitrarily, we take this distance to be unity. During mixing the following diffusion processes take place in B-side: i) volume diffusion along x-direction: A atoms enter directly from the interface into the grains of the B layer by volume diffusion; ii) GB diffusion along x-axis: by means of grain boundary transport A atoms fill the GBs of the B film; iii) volume diffusion of A atoms from the GBs into the bulk along the y-axis: GBs become a source of A atoms.

The concentration evolution obeys the following equations:

$$\frac{\partial c}{\partial t} = D_V \left(\frac{\partial^2 c}{\partial x^2} + \frac{\partial^2 c}{\partial y^2} \right) \tag{3a}$$

$$\frac{\partial c_{gb}}{\partial t} = D_{gb} \frac{\partial^2 c_{gb}}{\partial x^2} + \frac{2D_V}{\delta} \frac{\partial c}{\partial y}\bigg|_{y=\delta/2} \tag{3b}$$

The Eq. (3a) describes the volume diffusion in the grain, the Eq. (3b) gives the time evolution of the concentration in the boundary slab [31, 34]. Because of the regularly spaced GBs, the diffusion problem should be solved for the unit cell, (unit cell dimensions: $H \times (L/2 + \delta/2) \times 1$) shown as the shaded area in the Fig. 7. The chosen unit cell composed of a half-grain ($L/2 \times H$) and a 'half' grain boundary, is an appropriate one because the grain boundaries are symmetrical sources of material, i.e. the concentration profiles in the neighbouring grains should have a mirror symmetry (Fig. 8, stage III). It is worth to mention that in the model calculations it has no influence whether the GBs are continuous along the whole thickness or not, because of the unit cell for the calculation (shaded area on Fig. 7).

The following initial and boundary conditions were applied: initially the layers were mutually free from the atoms of the other layers. At the interface, $c(x = 0, t) = 0.5$ a constant concentration, c = 0.5 was maintained. At the topmost surface and at the substrate/film interface we supposed zero flux conditions:

$$\frac{\partial c(x,t)}{\partial x}\bigg|_{x=-H} = 0; \quad \frac{\partial c(x,t)}{\partial x}\bigg|_{x=H} = 0 \tag{4}$$

The plane in the middle of a grain (parallel to the GB slab at y = L/2) should be the mirror plane of the concentration distribution, and here the concentration should have a minimum, i.e. the zero flux condition can be assumed here as well:

$$\frac{\partial c}{\partial y}\bigg|_{y=L/2} = 0$$

The partial differential equation system can be solved by the method of finite differences, using explicit [35] or the alternating direction implicit [34] (ADI) schemes.

In the present calculations we used a two-dimensional grid, covering the unit cell, the grid size in both x and y directions, was $\Delta x = \Delta y = \delta/2$. The following input parameters were used: the volume diffusion coefficient, ($D_V = 1 \times 10^{-26}$ m²s⁻¹), the grain boundary diffusion coefficient ($D_{gb} = 1 \times 10^{-19}$ m²s⁻¹), the grain size, ($L = 5$ nm) and the thickness of the layers ($H = 10$ nm).

Since experimentally usually the average concentration versus depth profiles can be mapped, the calculated concentrations in the grid points $c(t, i\Delta x, j\Delta y)$ at a given time (t), should be averaged over the grid points which are located along the line parallel to the original interface ($i = $ const.). By means of such lateral averaging (along y-axis) we get the average concentration in a section at a given depth (x, measured from the interface) and having the thickness of Δx.

The time evolution of the average concentration profiles, as a function of the depth (x) are shown in Fig. 9a. In accordance with Fig. 8, the following 3 stages can be distinguished:

i) stage I: $0 \le t \le \frac{H^2}{4D_{gb}}$ there is an intensive grain boundary diffusion (where the upper limit was obtained from the GB penetration equal to H: $H = 2(D_{gb}t)^{1/2}$), causing a time dependent initial slope at the original interface (see also Table 3, at $5s \le t \le 500s$); if $t \approx \frac{H^2}{D_{gb}}$ GBs become saturated, because of the boundary conditions specified at $\pm H$ (Eq. (4)).
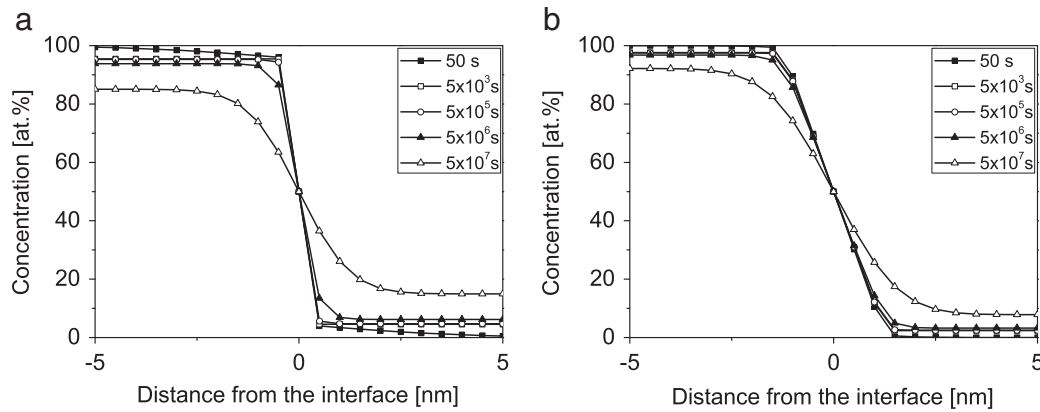
Fig. 9. Time evolution of the concentration calculated numerically in a nanocrystalline bilayer film in the region of -5 nm < 0 < 5 nm; as for the input parameters see the text. The concentration as a function of the distance measured from the interface is plotted in (a) for the ideal case. In order to simulate the finite depth resolution of an experimental method, the profiles were also smoothed using a 5-point moving average procedure in (b). The annealing times are shown in the inset, as for the slopes and diffusion coefficients, see also Table 3.

ii) stage II: in the time interval determined by the relation $\frac{H^2}{D_{gb}} \leq t \leq \frac{\delta^2}{2D_v}$, the average concentration profiles remain practically unchanged, since the grain boundary concentrations are constant, the concentrations in the grain, even in the first section (at x = 0.5 nm) remains very small because of the negligible volume diffusion. Therefore the average concentration in a section will be determined by the concentration in the GBs (see Table 3, at t = 5×10³-1×10⁵s). Supposing 5-10% GB fraction, the average concentration is well detectable experimentally.

iii) stage III: if $t \geq \frac{\delta^2}{2D_v}$ is fulfilled, the concentrations inside the grain grid points become comparable with the concentrations in the GBs, so the average concentration in the sections is determined by the volume diffusion (see Table 3, at t≥1×10⁵ s).

Essentially, in the above classification stage I and stage II correspond to the Harrison's C-regime, stage III corresponds to the B kinetic regime.

The maximum bulk penetration length in our case was less than 2 nm (Table 3); i.e. the finite thickness of the film (reflection from the outer surfaces) has no effect on the slopes. Therefore the thickness of the film would play a role only if the bulk penetration length is comparable to H i.e. at small values of H, comparable with the bulk penetration length (<2 nm).

In order to demonstrate the effect of the non-ideal depth resolution of the experimental profiling techniques, we additionally smoothed the calculated concentration data using a 5-point moving average procedure (Fig. 9(b) and Table 3). This averaging procedure

takes place along the x-axis and it smoothes the data by replacing each data point with the average of the 5 neighbouring points. The slopes of such "smoothed" profiles at the interface become smaller; consequently, the evaluated diffusion coefficients are higher, indicating that the evaluated diffusion coefficients may also depend on the experimental method. Thus Fig. 9a and b represent curves provided by a device with 'ideal' as well as with 'real' (smoothed) depth resolution, respectively. In stage I, until the condition $2 \times \sqrt{D_v t} << \delta$ is fulfilled (C-type kinetic regime), the gradual saturation of GBs takes place. The diffusion coefficients were evaluated from the slopes of the 'ideal' as well as 'real' profiles, using Eq. (2) and supposing a step-like initial profile $G_0^{-2} \approx 0$, i.e. the $D = (1/G^2)(1/4\pi t)$ relation was used for the calculation of the apparent diffusion coefficients (denoted in Table 3 as D_{id}, D_{real}, respectively). It can be seen from Table 3 that the deduced coefficients at short annealing times have almost the same orders of magnitude as the input GB diffusion coefficient. Having increased the bulk penetration depth, (moving to the B-type kinetic regime) the apparent diffusion coefficients become closer and closer to the input value of the volume diffusion coefficient. The stage II, can be considered as a transition regime.

In order to separate the competing effects we can also treat the profiles as a result of a two-step annealing process. The first step is characterized by the parameters t_1, G_1, (parameters of the previous 'parent' profile) and the second step with t_2, G_2 parameters (parameters of the actual profile). On the basis of Eq. (2) the diffusion coefficients can be evaluated from the slopes calculated at x = 0, applying the above

Table 3
The diffusion parameters evaluated from the calculated profiles shown in Fig. 9. The parameter G is the initial slope of the profiles in the neighbourhood of the interface, D_{id} as well as D_{real} are the apparent diffusion coefficients, without (Fig. 9a) and with averaging (Fig. 9b), while D'_{real} were obtained from Eq. (5): see also the text. (Input parameters: $D_V = 1 \times 10^{-26}$ m²s⁻¹, $D_{gb} = 1 \times 10^{-19}$ m²s⁻¹, δ=0.5 nm, L = 5 nm, H = 10 nm).

Annealing time [s]	$2\sqrt{D_v t}$ [nm]	Parameters determined from the calculated profile		Parameters determined from the smoothed profile		
		G [1/nm]	D_{id} [m²/s]	G [1/nm]	D_{real} [m²/s]	D'_{real} [m²/s]
5	4.5×10^{-4}	0.944	1.8×10^{-20}	0.392	1.0×10^{-19}	–
50	1.4×10^{-3}	0.921	1.9×10^{-21}	0.375	1.1×10^{-20}	1.1×10^{-21}
500	4.5×10^{-3}	0.912	1.9×10^{-22}	0.366	1.2×10^{-21}	6.3×10^{-23}
5×10^3	1.4×10^{-2}	0.909	1.9×10^{-23}	0.364	1.2×10^{-22}	1.5×10^{-24}
2×10^4	2.8×10^{-2}	0.908	4.8×10^{-24}	0.364	3.0×10^{-23}	0
5×10^4	4.5×10^{-2}	0.907	1.9×10^{-24}	0.364	1.2×10^{-23}	0
1×10^5	6.3×10^{-2}	0.905	9.7×10^{-25}	0.363	6.0×10^{-24}	3.3×10^{-26}
5×10^5	1.4×10^{-1}	0.888	2.0×10^{-25}	0.362	1.2×10^{-24}	1.3×10^{-26}
1×10^6	2.0×10^{-1}	0.867	1.1×10^{-25}	0.361	6.1×10^{-25}	6.7×10^{-27}
5×10^6	4.5×10^{-1}	0.731	2.9×10^{-26}	0.348	1.3×10^{-25}	1.2×10^{-26}
1×10^7	6.3×10^{-1}	0.609	2.1×10^{-26}	0.330	7.3×10^{-26}	1.5×10^{-26}
5×10^7	1.4	0.270	2.2×10^{-26}	0.216	3.4×10^{-26}	2.4×10^{-26}

multistep annealing procedure:

$$D' = \left(\frac{1}{G_2^2} - \frac{1}{G_1^2}\right)\frac{1}{(4\pi(t_2-t_1)} \tag{5}$$

In Table 3 the values of D'_{real}, were calculated from the smoothed profiles (shown in Fig. 9b), using Eq. (5).

The time dependence of the D' (Fig. 10) shows that in real experiments one can get reliable volume diffusion data only if the condition $2\sqrt{D_v t} > \delta$ is strictly fulfilled. On the other hand, if we use Eq. (5) to evaluate the diffusivity from the smoothed profiles (Fig. 9b), we can even underestimate the diffusion coefficients, since there could exist a certain annealing time interval in which there is no change in the slope, resulting near zero value for D'_{real} (see the last column in Table 3 at 5×10^5 s time). This corresponds to the situation when the composition distribution in the GB's became practically homogeneous but still there was no penetration to the bulk.

In order to check that the time dependence of the diffusion coefficient indeed behaves similarly as predicted from the above model we applied an additional heat treatment on the sample annealed at 773 K. After 9000 s it was obtained that the diffusion coefficient was about one and half order of magnitude lower (8.61×10^{-23} m²s⁻¹) than the value shown in Table 2 for this temperature. The point corresponding to this value is also shown in Fig. 4. Thus the above value is in good agreement with the model presented above and also correlates with the results obtained by Chakravarty et al. [4].

As a general conclusion we observe that special attention is needed in these studies if one is to draw unequivocal conclusions as to the reasons for the low activation energies obtained for diffusion. We do not dispute that effects mentioned in the interpretation of the results of previous works [4,5] (i.e. the grain boundary transport can be neglected, mechanisms of point defect annihilation at the interface [4] or special strongly correlated diffusion [5]), are present. However our results indicate that the presence of rapid diffusion paths in nanofilms – such as triple junctions, grain boundaries or dislocations – is very important in experiments with very short annealing times and corresponding small diffusion lengths. Care is necessary to separate these effects from other contributions to bulk diffusion or defect relaxation.
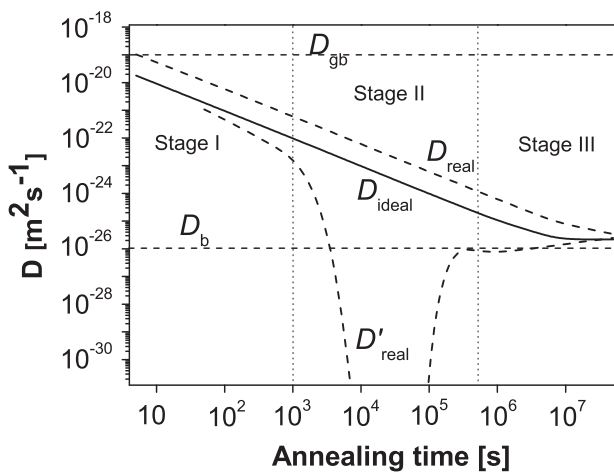
5. Conclusions

Self-diffusion of Fe in thin films of Pt/^{56}Fe/^{57}Fe grown on MgO (100) was studied. Effective self-diffusion coefficients for Fe were determined in the temperature range 703 K to 813 K with an activation energy 1.54 ± 0.25 eV.

Deep penetration of the Pt into the ^{56}Fe layer was also observed, which indicated the occurrence of GB diffusion. The grain boundary diffusion coefficients of Pt were also determined in the above temperature range and an activation energy of 1.45 ± 0.25 eV was deduced from the Pt concentration profiles.

Since in our samples columnar grains of about 10-30 nm diameter were observed we interpreted our results for Pt diffusion as diffusion along tilt grain boundaries.

The results demonstrate that the presence of grain boundaries has an influence on intermixing caused by the Fe self-diffusion–since the activation energy of it was very close to the value obtained for Pt grain boundary diffusion. Model calculations illustrate that in nanostructured thin film diffusion couples the initial decrease of the sharpness of composition profile can be controlled by grain boundary diffusion and only at much longer annealing times – when the composition profiles in the grain boundaries have been already almost fully homogenized – the bulk diffusion controls the intermixing. Thus our results indicate that the presence of rapid diffusion paths in nanofilms is very important in experiments with very short annealing times and corresponding small diffusion lengths. Care is necessary to separate these effects from other contributions to bulk diffusion or defect relaxation.

References

[1] H. Natter, M. Schmelzer, M.S. Löffler, C.E. Krill, A. Fitch, R. Hempelmann, Grain-Growth Kinetics of Nanocrystalline Iron Studied In Situ by Synchrotron Real-Time X-ray Diffraction, J. Phys. Chem. B 104 (2000) 2467.
[2] R. Würschum, S. Herth, U. Brossmann, Diffusion in Nanocrystalline Metals and Alloys—A Status Report, Adv. Eng. Mater. 5 (2003) 365.
[3] Y. Estrin, G. Gottstein, E. Rabkin, L.S. Shvindlerman, Grain growth in thin metallic films, Acta Mater. 49 (2001) 673.
[4] S. Chakravarty, H. Schmidt, U. Tietze, D. Lott, N.P. Lalla, A. Gupta, Self-diffusion and defect annihilation in nanocrystalline Fe films probed by neutron reflectometry, Phys. Rev. B 80 (2009) 014111.
[5] M. Rennhofer, B. Sepiol, M. Sladecek, D. Kmiec, S. Stankov, G. Vogl, M. Kozlowski, R. Kozubski, A. Vantomme, J. Meersschaut, D. Rüffer, A. Gupta, Self-diffusion of iron in L10-ordered FePt thin films, Phys. Rev. B 74 (2006) 104301.
[6] G. Hettich, H. Mehrer, K. Maier, Self-diffusion in ferromagnetic α-iron, Scr. Metall. 11–9 (1977) 795.
[7] C.M. Walter, N.L. Peterson, Isotope Effect in Self-Diffusion in Iron, Phys. Rev. 178 (1969) 922.
[8] M. Lübbehusen, H. Mehrer, Self-diffusion in α-iron: The influence of dislocations and the effect of the magnetic phase transition, Acta Metall. Mater. 38 (1990) 283.
[9] Y. Iijima, K. Kimura, K. Hirano, Self-diffusion and isotope effect in α-iron, Acta Metall. 36 (1988) 2811.
[10] H. Tamimoto, P. Farber, R. Würschum, R.Z. Valiev, H.-E. Schaefer, Self-diffusion in high-density nanocrystalline Fe, Nanostruct. Mater. 12 (1999) 681.
[11] S.V. Divinski, J. Geise, E. Rabkin, C. Herzig, Grain boundary self-diffusion in α-iron of different purity: effect of dislocation enhanced diffusion, Z. Metallkd. 95 (2004) 945.

Fig. 10. Time dependence of the effective diffusion coefficients calculated from the profiles shown in Fig. 9 and given in Table 3 (D_{ideal} - determined from the calculated profiles in Fig. 9a, D_{real} - determined from the smoothed profile (9b) and D'_{real} - calculated from the smoothed profile using Eq. (5)). The corresponding time intervals of Stages I-III (see Fig. 8) are also indicated.

[12] H. Schmidt, S. Chakravarty, M. Jiang, E. Hüger, P.K. Parida, T. Geue, J. Stahn, U. Tietze, D. Lott, Grain boundary self-diffusion in Fe films with a stable nanostructure, J. Mater. Sci. 47 (2012) 4087.

[13] H. Mehrer (Ed.), , Diffusion in Solid Metals and Alloys, Landolt Börstein (New Series), vol. lII/26, Springer, Berlin, 1990.

[14] M. Gupta, A. Gupta, S. Rajagopalan, A.K. Tyagi, Self-diffusion of iron in amorphous iron nitride, Phys. Rev. B 65 (2002) 214204.

[15] A. Gupta, M. Gupta, U. Pietsch, S. Ayachit, S. Rajagopalanl, A.K. Balamurgan, A.K. Tyagi, Iron self-diffusion in nanocrystalline FeZr thin films, J. Non-Cryst. Solids 343 (2004) 39.

[16] M. Gupta, A. Gupta, S. Chakravarty, T. Gutberlet, Iron Self-Diffusion in Chemically Homogeneous Multilayers, Defect Diffus. Forum 237–240 (2005) 548.

[17] L.G. Harrison, Influence of dislocations on diffusion kinetics in solids with particular reference to the alkali halides, Trans. Faraday Soc. 57 (1961) 1191.

[18] M. Vasylyev, S. Sidorenko, S. Voloshko, V. Kostiuchenko, I. Kotenko, Low Temperature Self-Diffusion of Iron in the ^{56}Fe/^{57}Fe Stable-Isotope Thin-Film System, Defect Diffus. Forum 261–262 (2007) 85.

[19] J. Jorzick, J. Lösch, M. Kopnarski, H. Oechsner, Detection in the ppm range and high-resolution depth profiling with the new SNMS instrument INA-X, Appl. Phys. A Mater. Sci. Process. 78 (2004) 655.

[20] L. Péter, G.L. Katona, Z. Berényi, K. Vad, G.A. Langer, E. Tóth-Kádar, J. Pádár, L. Pogány, I. Bakonyi, Electrodeposition of Ni–Co–Cu/Cu multilayers, Electrochim. Acta 53 (2007) 837.

[21] M. Ibrahim, Z. Balogh, P. Stender, R. Schlesiger, G.-H. Greiwe, G. Schmitz, B. Parditka, G.A. Langer, A. Csik, Z. Erdélyi, Acta Mater. 76 (2014) 306.

[22] M. Ibrahim, B. Parditka, A. Fuhrich, Z. Balogh, P. Stender, Z. Erdélyi, G. Schmitz, Phys. Status Solidi C 10 (2013) 1724.

[23] H.G. Tompkins, M.R. Pinnel, Low-temperature diffusion of copper through gold, J. Appl. Phys. 47 (1976) 3804.

[24] J.E.E. Baglin, J.M. Poate, in: J.M. Poate, K.N. Tu, J.W. Mayer (Eds.), Thin Films-Interdiffusion and Reactions, Wiley, New York 1978, p. 407.

[25] J.M. Poate, P.A. Turner, W.J. DeBonte, J. Yahalom, Thin-film interdiffusion. I. Au-Pd, Pd-Au, Ti-Pd, Ti-Au, Ti-Pd-Au, and Ti-Au-Pd, J. Appl. Phys. 46 (1975) 4275.

[26] P.M. Hall, J.M. Morabito, A formalism for extracting diffusion coefficients from concentration profiles, Surf. Sci. 54 (1976) 79.

[27] P.M. Hall, J.M. Morabito, J.M. Poate, Diffusion mechanisms in the Pd/Au thin film system and the correlation of resistivity changes with Auger electron spectroscopy and Rutherford backscattering profiles, Thin Solid Films 33 (1976) 107.

[28] U. Pietsch, V. Holy, T. Baumbach, High-Resolution X-Ray Scattering, 2nd ed. Springer-Verlag, New York, 2004. 408.

[29] J. Chakraborty, U. Welzel, E.J. Mittemeijer, Interdiffusion, phase formation, and stress development in Cu–Pd thin-film diffusion couples: Interface thermodynamics and mechanisms, J. Appl. Phys. 103 (2008) 113512.

[30] H. Mehrer, M. Lübbehusen, Self-Diffusion along Dislocations and in the Lattice of alpha-Iron, Defect Diffus. Forum 66–69 (1989) 591.

[31] I. Kaur, Y. Mishin, W. Gust, Fundamentals of Grain and Interphase Boundary Diffusion, Wiley, Chichester, 1988.

[32] I.A. Szabó, D.L. Beke, On the transition between the C- and B-kinetics regimes for grain-boundary diffusion, Philos. Mag. A 62 (1990) 227.

[33] G.L. Katona, I.A. Vladymyrskyi, I.M. Makogon, S.I. Sidorenko, F. Kristály, L. Daróczi, A. Csik, A. Liebig, G. Beddies, M. Albrecht, D.L. Beke, Appl. Phys. A 115 (2014) 203.

[34] G.H. Gilmer, H.H. Farrel, Grain-boundary diffusion in thin films. II. Multiple grain boundaries and surface diffusion, J. Appl. Phys. 47 (1976) 4373.

[35] A. Makovec, G. Erdélyi, D.L. Beke, Grain boundary diffusion in thin films with a bimodal grain boundary structure, Thin Solid Films 520 (2012) 2362.